Soft Matter

PAPER

View Article Online
View Journal

Cite this: DOI: 10.1039/d1sm01638e

Synthesis of nanostructured protein–mineral-microcapsules by sonication†

Ulrike Doering,[a] Dmitry Grigoriev, *[b] Kosti Tapio,[ac] Ilko Bald [a] and Alexander Böker [b]

We propose a simple and eco-friendly method for the formation of composite protein–mineral-microcapsules induced by ultrasound treatment. Protein- and nanoparticle-stabilized oil-in-water (O/W) emulsions loaded with different oils are prepared using high-intensity ultrasound. The formation of thin composite mineral proteinaceous shells is realized with various types of nanoparticles, which are pre-modified with Bovine Serum Albumin (BSA) and subsequently characterized by EDX, TGA, zeta potential measurements and Raman spectroscopy. Cryo-SEM and EDX mapping visualizations show the homogeneous distribution of the densely packed nanoparticles in the capsule shell. In contrast to the results reported in our previous paper,[1] the shell of those nanostructured composite microcapsules is not cross-linked by the intermolecular disulfide bonds between BSA molecules. Instead, a Pickering-Emulsion formation takes place because of the amphiphilicity-driven spontaneous attachment of the BSA-modified nanoparticles at the oil/water interface. Using colloidal particles for the formation of the shell of the microcapsules, in our case silica, hydroxyapatite and calcium carbonate nanoparticles, is promising for the creation of new functional materials. The nanoparticulate building blocks of the composite shell with different chemical, physical or morphological properties can contribute to additional, sometimes even multiple, features of the resulting capsules. Microcapsules with shells of densely packed nanoparticles could find interesting applications in pharmaceutical science, cosmetics or in food technology.

Received 17th November 2021,
Accepted 8th March 2022

DOI: 10.1039/d1sm01638e

rsc.li/soft-matter-journal

Introduction

Over the course of the last two decades, several methods for the synthesis of microcapsules with shells of various materials were presented. The capsules have been prepared from self-assembled biomolecules[2,3] through layer-by-layer (LbL)-assembly,[4–6] or by using emulsion droplets as template.[7–9] These droplets can be stabilized by proteins[1] or nanoparticles (NPs) forming so-called Pickering emulsions.[9–11] An emulsion has the advantages of a one-pot synthesis and of the possibility to control the size of the droplets and therefore of the resulting capsules. Those capsules are used for the encapsulation of various compounds, such as nutrients,[12] fragrances,[13] pharmaceuticals[14] and catalysts.[15]

The choice of the wall material is an important aspect of the capsules. Inorganic materials can endure higher temperatures and exhibit higher rigidity. The novel physical features created by the formation of a densely packed spherical shell from colloidal building blocks have attracted increasing interest. Most commonly used materials in the scientific fields of biomedicine are calcium carbonate,[16] calcium phosphate[7,9] and silica.[8,10] The choice of colloids can control the physical characteristics of the microcapsules, including biocompatibility, permeability and mechanical strength. Then again, biopolymers as wall material have the benefit that their properties can be adjusted with the possibility to make them stimuli-responsive enabling a controlled release of loaded substances.[2,17,18] Further benefits are their biodegradability, natural abundance and low costs.

Proteins have also been thoroughly examined as biological building blocks for capsule shells. They offer various advantages with their structural and chemical versatility, amphiphilic character and emulsifying properties.[19] Suslick and Grinstaff developed a technique for the synthesis of protein microcapsules using ultrasound.[20] First, the ultrasonic treatment of a two-phase liquid system takes place resulting in an oil-in-water (O/W) emulsion stabilized by protein molecules, which cross-link at the interface *via* disulfide bonds. This cross-linking is initiated by the superoxide radicals created from the ultrasound energy leading to oil loaded protein microcapsules. With this technique, microcapsules with various proteins and controllable sizes can be synthesized.[21–25]

[a] University of Potsdam, Institute of Chemistry, Karl-Liebknecht-Str. 24-25, 14476, Potsdam, Germany
[b] Fraunhofer Institute for Applied Polymer Research IAP, Geiselbergstr. 69, 14476 Potsdam, Germany. E-mail: dmitry.grigoriev@iap.fraunhofer.de
[c] University of Jyväskylä, Department of Physics and Nanoscience Center, P.O. Box 35, Fi-40014 Jyväskylä, Finland

† Electronic supplementary information (ESI) available. See DOI: 10.1039/d1sm01638e

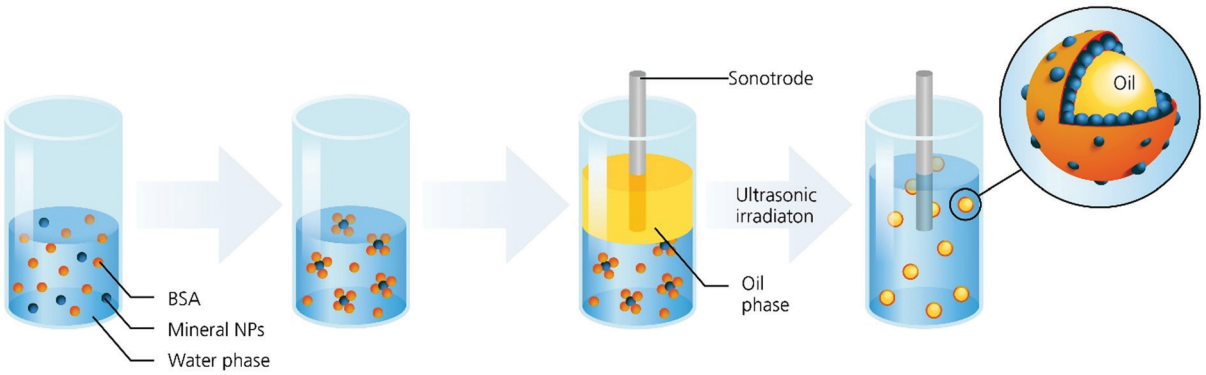

Fig. 1 Synthesis scheme of oil loaded composite BSA microcapsules.

The combination of inorganic nanoparticles and proteins will enable the synthesis of new hybrid materials.[7,26,27] Here, we present a fast and economic method for the formation of composite protein-mineral-microcapsules induced by sonication in an one-pot-process. Using high-intensity ultrasound protein- and nanoparticle-stabilized (O/W) emulsions loaded with different oils were synthesized. Silica, calcium carbonate and hydroxyapatite (HAP) nanoparticles were used for the formation of the composite microcapsules. The schematical illustration of the synthesis of composite protein microcapsules is given in Fig. 1.

Experimental

Materials

Bovine serum albumin (BSA, >95%) and 3-Aminopropyltriethoxysilane (APTES, 97%) were purchased from Alfa Aesar (Germany). Toluene (≥99.5%) and ethanol (≥99.5%) were purchased from Th. Geyer (Germany), Miglyol 812 was purchased from Sasol (Germany) and mint oil was purchased from Hofmann und Sommer GmbH (Germany). BisTris (≥99%) buffer solution and dimethylsulfoxid (DMSO, (≥99,8%)) were purchased from Carl Roth (Germany). Diammonium hydrogen phosphate and calcium nitrate tetrahydrate (≥99%) was purchased from VWR (Germany). Ammonium hydroxide (28–30%) was purchased from Merck (Germany). The aqueous Ludox Cl suspension (aluminum oxide coated silica NPs, 30% w/v) was purchased from Sigma Aldrich (Germany), dry silica particles, whose surface was partially modified with DCDMS (71% of surface silanol groups remained intact) and called as Si71 were purchased from Wacker GmbH (Germany) and calcium carbonate NPs, whose surface was modified with stearic acid, was purchased from GetNanoMaterials (France). Fluorescein isothiocyanate (FITC) was obtained from Riedel-de Haën (Germany).

Synthesis of HAP NPs

A diammonium hydrogen phosphate solution (10 mM) was adjusted to pH = 9 with small amounts of ammonium hydroxide solution (1%). A calcium nitrate solution (20 mM) was added to an equal volume of the diammonium hydrogen phosphate solution while it was sonicated at an acoustic power of ∼100 W cm^{-2}. The obtained nanoparticle suspension was concentrated by centrifugation and redispersed with a BisTris solution (20 mM, pH = 7).

Synthesis of composite protein microcapsules

In the first step, the NPs were pre-modified with BSA. For this purpose, a NP suspension (1% w/v) in distilled water (Ludox Cl, Si71, $CaCO_3$ or HAP) was added dropwise to an equal volume of a BSA solution (5% w/v) in distilled water with pH 6.7. After thorough washing process including multistep washing and subsequent centrifugation at 14 000 rpm, the BSA modified NPs were redispersed with a BisTris solution (20 mM, pH = 7). The stearic acid covered $CaCO_3$ NPs were hydrophilized before the pre-modification with BSA by adding NaOH (1 mL, 0.1 M) and Na_3PO_4 (1 mL, 0.1 M) to $CaCO_3$ (100 mg) in distilled water (10 mL) and sonicating the mixture for 1 min. In a cylindrical vessel, oil (1.4 mL toluene, Miglyol or mint oil) was layered over a BSA modified NP suspension (2.1 mL). A high-intensity ultrasonic horn with a tip diameter of 3 mm was placed at the oil–water interface. To maintain the temperature below 30 °C during ultrasonication, the vessel was positioned in an ice bath. The systems were sonicated for 3 minutes, except for the Ludox Cl samples that were sonicated for 1 min, at an acoustic power of ∼200 W cm^{-2}. Simultaneously, the systems were mixed with a magnetic stirrer.

Fluorescent labelling

FITC (1 mg mL^{-1}) was dissolved in DMSO. The FITC solution (210 μL) was added to the emulsion (3.5 mL) containing the composite capsules. The resulting solution was mixed by manual shaking and stored over night at 4 °C in the dark for reaction.

Modification with APTES, FITC and RITC

The Ludox Cl NPs (1% w/v) were dispersed in ethanol (5 mL). To remove residual water the solution was centrifuged at 10 000 rpm and redispersed with an equal volume of ethanol. Subsequently, ammonium hydroxide solution (30%, 0.167 mL) and APTES (0.06 M, 900 μL) in ethanol were slowly added while the suspension was mixed with a magnetic stirrer. The mixture was continuously stirred overnight (*ca.* 16 h). After further centrifugation and redispersing in ethanol, FITC solution (0.5 mg mL^{-1}, 60 μL) in DMSO was added and the mixture

was stored at 4 °C for 2 h. The suspension was centrifuged again and then redispersed with BisTris buffer solution (2.5 mL, 20 mM, pH = 7). Thereafter, a RITC labelled BSA solution (5% w/v, 2.5 mL) was added, the mixture was once more centrifuged and redispersed with BisTris (2.5 mL). Finally, the synthesis of the oil loaded composite protein microcapsules was carried out as described previously.

Thermogravimetric analysis

The thermal stability of the samples was measured by means of thermogravimetric analysis (TGA) with a TGA2 LF/1100/885 from Mettler. Each sample was heated from 30 to 700 °C, except for the hydrophilized $CaCO_3$ that was heated up to 800 °C, at a heating rate 10 °C min^{-1} under air atmosphere.

Zeta potential measurements

The zeta potential of the APTES and FITC modified Ludox Cl NPs was measured with a Malvern Zetasizer Nano ZS possessing a red 632.8 nm laser.

Cryo scanning electron microscopy

Characterization with cryo scanning electron microscopy was done on two devices, on a S-4800 (Hitachi SEM, Japan) instrument and a 7500F (Jeol SEM, Japan) one.

Energy dispersive X-ray

EDX spectra were recorded with a Xmax 150 and Xmax 80 (Oxford) mounted on the Jeol 7500F.

Raman spectroscopy

All Raman data was acquired using a Witec Alpha 300 Raman microscope system (Witec, Ulm, Germany) equipped with a spectrograph (600 g mm^{-1} grating) and an Andor DU401A-BR-DD-352 CCD camera (Andor, Concord, Massachusetts, USA). 488 nm excitation laser was utilized during the measurements. Before measurements, the power density was adjusted to 3.7×10^4 W cm^{-2} for the 488 nm laser (the estimated spot size is 1.32 μm). The dried samples were placed on empty microscope slides and slightly pressed and flattened using a spatula. Slides were put under the microscope and the signal was acquired by measuring single point spectra from different areas. The dried BSA sample was measured using 12 s integration time and averaging over 20 spectra, the dried BSA–toluene-capsule sample with 8 s and 30 spectra averaging, the Ludox Cl sample with 1 s and 100 spectra averaging, the BSA modified Ludox Cl and the dried BSA-Ludox Cl–toluene-capsule samples with 5 s and 100 spectra averaging. The Si71, the BSA modified Si71, the HAP and the BSA modified HAP samples were measured using 5 s integration time and averaging over 60 spectra.

Results and discussion

Characterization of the modified nanoparticles

Coating the NPs with BSA enables their ability to stabilize (O/W) emulsions and thereby the formation of composite protein-mineral microcapsules. HAP, Ludox Cl silica particles, whose surface was partially modified with dichlorodimethylsilane (DCDMS) and called from now on as Si71 as well as calcium carbonate NPs were characterized with TGA, Zetasizer, SEM, EDX and Raman spectroscopy.

Fig. 2 shows how the ZP of BSA, Ludox Cl and HAP changes at different pH values and the zeta potential values of pristine and BSA modified nanoparticles are listed in Table 1.

As reported in the literature the isoelectric point (IEP) of BSA is at pH 4.7[28] and above this pH value, BSA is negatively charged. In contrast, the Ludox Cl NPs have a strongly positive charge, which is the perfect precondition for the adsorption of BSA due to the electrostatic attraction between those positively charged particles and the negatively charged protein molecules. After the addition of BSA and a thorough washing process including multistep washing and subsequent centrifugation, the zeta potential of the Ludox Cl NPs with adsorbed BSA was reversed and had an equivalent zeta potential to BSA with a value of −19.8 mV at pH 6.6, showing that the adsorption was successful. In the investigated pH range from 5.8–7.2 the synthesized HAP NPs have a negative zeta potential as well as Si71 and $CaCO_3$ (hydrophilized) at pH 7 and 7.4, respectively. The IEP of $CaCO_3$ is usually at pH 8.9 and therefore the ZP at pH 7.4 should be positive.[29,30]

This shows that the hydrophilization of the $CaCO_3$ NPs by sonication did not completely remove the stearic acid on the surface. However, after the adsorption of BSA the zeta potential of the modified HAP, Si71 and $CaCO_3$ NPs shows a slight shift in the direction of the value of pristine BSA. Since these NPs are not oppositely charged to BSA, the electrostatic attraction cannot be considered to be the driving force for the adsorption of the protein molecules. The protein adsorption is the result of various interactions between the components, not only electrostatic forces but also van der Waals forces, hydrogen bonding and hydrophobic interactions.[31] Nevertheless, in particular

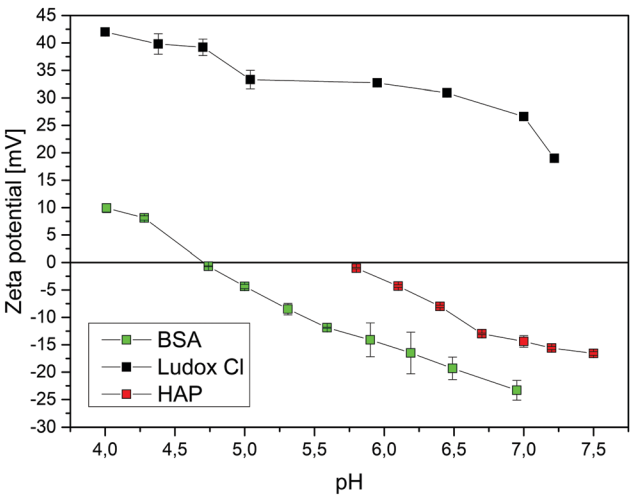

Fig. 2 Zeta potential measurements of BSA, Ludox Cl and HAP at different pH values.

Table 1 List of zeta potential values of pristine and BSA modified nanoparticles

Nanoparticles	pH	Zeta potential [mV]
BSA	6.5	−19.3 ± 2.1
BSA	7.0	−23.3 ± 1.8
Ludox Cl	6.5	+30.9 ± 0.5
BSA + Ludox Cl	6.6	−19.8 ± 0.4
HAP	7.0	−14.4 ± 1.1
BSA + HAP	7.0	−16.9 ± 0.4
Si71	7.0	−33.2 ± 0.1
BSA + Si71	7.0	−26.3 ± 0.1
$CaCO_3$ (hydrophilized)	7.4	−15.3 ± 1.3
BSA + $CaCO_3$	7.4	−25.1 ± 1.0

cases like with Ludox Cl, the electrostatic forces clearly dominate the adsorption of BSA at the solid/water interface.

The TGA measurements were used to determine the adsorption of BSA on the surface of various NPs and the composition of those modified particles (Fig. 3). The TGA curve of the pristine BSA is displayed in all TGA diagrams for better comparison. A three-step decomposition curve can be observed for the pristine BSA. The initial weight loss at 100 °C is assigned to the dehydration of the sample. The weight loss of BSA started when the temperature rises above 200 °C. The third step is starting at approximately 450 °C and ends at 600 °C. The total weight loss was 97.5 wt% demonstrating that BSA decomposes completely in this temperature range.

The black curve in Fig. 3 A belongs to the synthesized HAP and it shows a weight loss of 11 wt% as the temperature was increased to 700 °C because of the evaporation of the residue crystal water. The green curve of the BSA modified HAP NPs started with the degrading as pristine BSA at 200 °C and it stopped decomposing at 600 °C as well but with a weight loss of 75 wt%. Comparing the TGA curve of pristine BSA and HAP it is clear that the thermal decomposition of the amino acid residues of BSA and its peptide chains is responsible for this weight loss showing that the residual 25 wt% are attributed to HAP.

A similar behavior has been observed for the other NPs. The Ludox Cl particles exhibit a weight loss of 18 wt% (Fig. 3B) which is in the same range as the weight loss of HAP, while the weight loss of the BSA modified Ludox Cl particles is 44 wt%. The amount of the residual Ludox Cl with 56 wt% is more than twice as high as the residual HAP with 25 wt%.

The TGA curves for the pristine and the BSA modified Si71 particles are shown in Fig. 3C. No weight loss was observed in the TGA curve of the pristine Si71 particles, whereas the BSA modified NPs have a weight loss of 65 wt% leaving 35 wt% as residual silica particles.

Fig. 3D displays the thermal decomposition of the $CaCO_3$ NPs, that were hydrophilized by sonication and the same particles additionally modified with BSA. The decomposition begins when the temperature rises above 600 °C and ends at approximately 750 °C with a weight loss of 45 wt%. It decomposes to calcium oxide and carbon dioxide.[32,33] The BSA modified $CaCO_3$ NPs begin to decompose at 200 °C slightly faster than the pristine BSA.

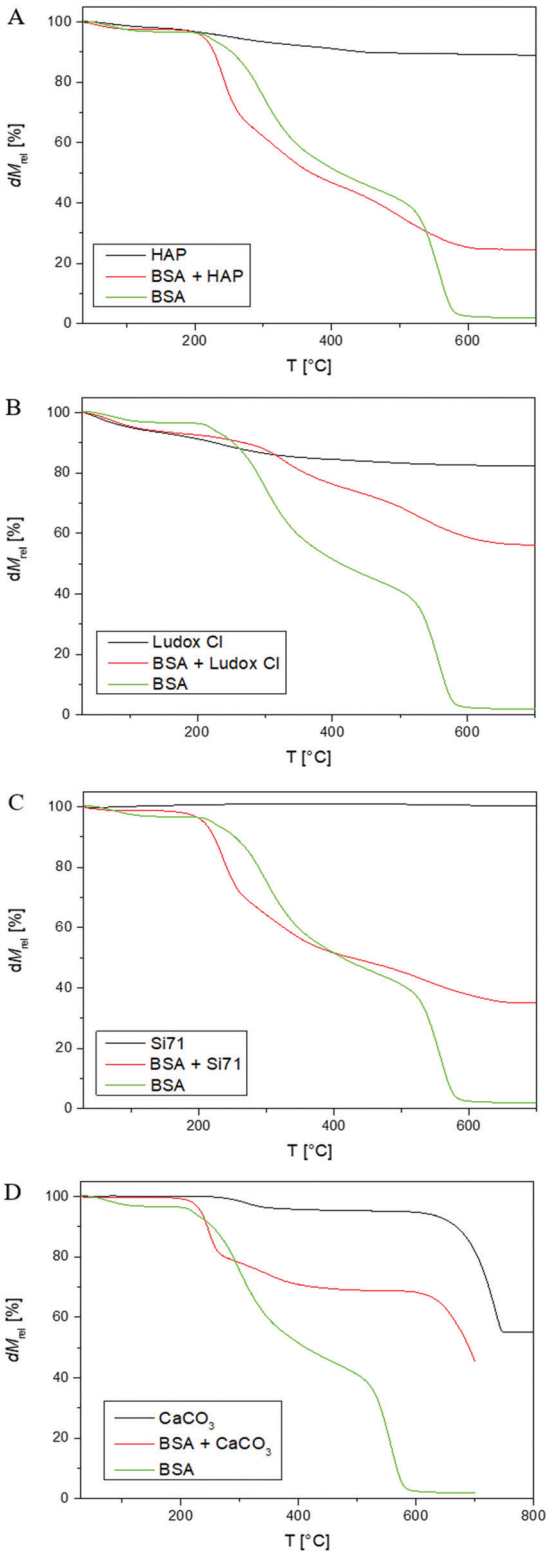

Fig. 3 TGA measurements of BSA adsorbed on HAP (A), Ludox Cl (B), Si71 (C) and $CaCO_3$ (D) measured in air atmosphere.

At 600 °C where BSA is fully degraded and before the decomposition of the $CaCO_3$ NPs starts, the residual mass is 68 wt%. The TGA measurements showed that BSA adsorbed

strongly on four different types of NPs and can be detected even after thorough washing process including multistep washing and subsequent centrifugation.

Notably, the adsorbed BSA decomposes faster than the pristine BSA. The TGA curve of the BSA modified Ludox Cl particles is the only sample where the adsorbed BSA decomposes slower than the pristine BSA, except from the beginning where the dehydration takes place. It is possible that this behavior is caused by the electrostatic attraction between BSA and Ludox Cl while the adsorption of BSA on the other NPs is driven by different interactions such as van der Waals forces, hydrogen bonding and hydrophobic interactions.

Moreover, the TGA curves show that the highest content of adsorbed BSA, which was amounted to 75 wt%, was found on the HAP NPs. The adsorption of BSA on HAP depends on the interaction of the anionic carboxyl group of the protein and the cationic calcium ions while the negative phosphate group follows a strong interaction with the positive amino group.[34,35] The TGA measurements indicates that these interactions could be stronger than the hydrophobic interactions between Si71 or $CaCO_3$ and BSA and the electrostatic attraction between Ludox Cl and BSA.

To obtain qualitative and quantitative information on the adsorption of BSA to the different NPs the energy dispersive x-ray spectroscopy (EDX) was performed. In Fig. 4a summary of the EDX measurements is given. Additionally, SEM images of the BSA modified NPs are shown on the left, while an overview of the elemental composition of the sample is displayed on the right.

The BSA modified Ludox Cl NPs consist mainly of oxygen with 53.8 wt% and silicon with 27.3 wt%. Furthermore, 4.5 wt% aluminum were detected, which is the evidence for the presence of Ludox Cl. In addition, 11.7 wt% carbon were detected confirming again the adsorption of BSA to the NPs like TGA and zeta potential measurements before. In contrast to the preparation for the capsule synthesis this sample was not washed with the BisTris buffer (pH = 7) to avoid an influence on the intensity of the carbon signal. Instead, the sample was washed with distilled water, whose pH was adjusted to 7 with a 0.001 M NaOH solution. Therefore, 0.6 wt% sodium were detected.

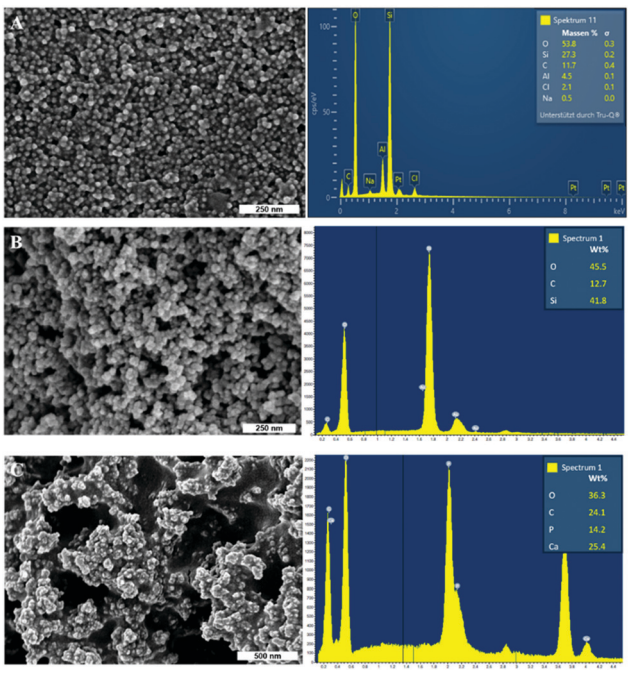

Fig. 4 SEM images and EDX analysis of BSA modified nanoparticles: Ludox Cl (A), Si71 (B) and HAP (C).

In the elemental composition diagram of the BSA modified Si71 NPs 45.5 wt% oxygen and 41.8 wt% silicon were detected. The amount of detected carbon is in the same range as in the Ludox Cl sample at 12.7 wt%.

14.2 wt% phosphorus and 25.4 wt% calcium were detected in the dried BSA modified HAP NPs. Notably, this sample contained the highest amount of carbon with 24.1 wt%. These results are in accordance with the TGA measurements.

To examine whether the adsorption of the BSA molecules to the NPs affects the protein conformation, the pristine and BSA modified NPs were additionally analyzed by Raman spectroscopy.

The results are shown in Fig. 5. BSA adsorbed on Ludox Cl and the pristine components are displayed in Fig. 5A. The spectrum of the BSA modified Ludox Cl NPs is basically the same as the pristine BSA spectrum. The additional peaks in this spectrum at 415 cm^{-1}, 747 cm^{-1}, 1077 cm^{-1} and 1266 cm^{-1} could be identified as buffer peaks caused by BisTris that was used during the washing process of the modified NPs to remove residual BSA, which was not adsorbed. Notably, the characteristic peak for the S–S vibration at 510 cm^{-1} is not present when BSA is adsorbed on the Ludox Cl NPs. Furthermore, the peaks of the amide I band at $\sim$1655 cm^{-1} and of the CH_2 and CH_3 bending at $\sim$1449 cm^{-1} were slightly shifted to $\sim$1665 cm^{-1} and $\sim$1460 cm^{-1} indicating that conformational changes take place when BSA adsorbs on the Ludox Cl NPs.[36] The bands that are typical for silica materials are only shown in the Raman spectrum of the pristine Ludox Cl particles. The bands at 250–650 cm^{-1} and 760–1100 cm^{-1} are attributed to the SiO_4 ring bending and Si–O stretching vibrational modes, respectively.[37] A CD study made by Giacomelli and Norde showed that the α-helix content of BSA decreased after adsorption on silica particles from 58% to 50%. The β-sheet content decreased as well by 8% while the unordered portion increased by 16%.[38] This study confirms that BSA changes its conformation upon adsorption on silica particles.

In Fig. 5B, the same peak shift can be observed in the spectrum of the BSA modified Si71 NPs. In contrast to the spectrum of the BSA modified Ludox Cl NPs, the characteristic peak of Si71 at $\sim$500 cm^{-1} can also be found in the spectrum after the adsorption of BSA. So, we can conclude that the BSA adsorption is much more effective on Ludox Cl resulting in a shielding of Raman scattering from Ludox Cl by BSA.

As discussed before, the Si71 NPs have a negative zeta potential, consequently the adsorption was not caused by electrostatic attraction. However, Norde and Favier proposed

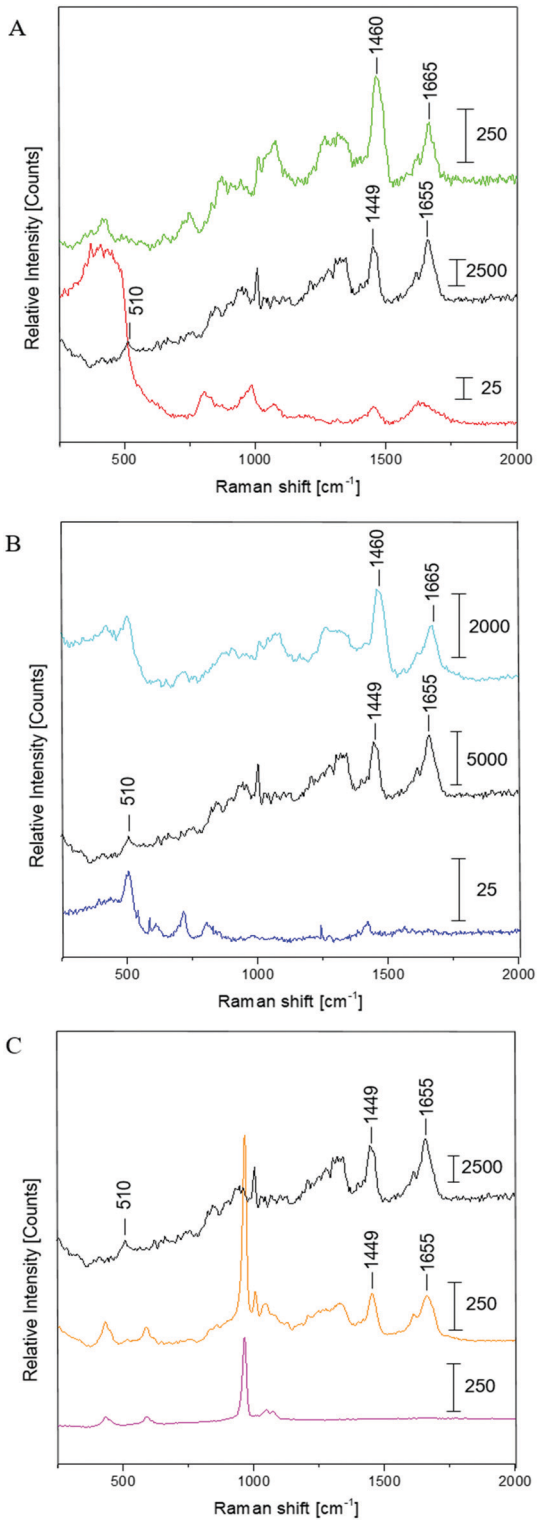

Fig. 5 Raman spectra for: (A) pristine BSA (black), pristine Ludox Cl (red), BSA modified Ludox Cl (green), (B) pristine Si71 (blue), BSA modified Si71 (light blue) and (C) pristine HAP (magenta) and BSA modified HAP (orange).

that the decrease in ordered structure would be the driving force for the adsorption of negatively charged BSA molecules on negatively and hydrophilic silica surfaces.[39]

The Raman spectrum of BSA adsorbed to HAP NPs is depicted in Fig. 5C. The characteristic peaks of BSA and HAP are clearly recognizable and in contrast to the spectra of the BSA modified silica NPs, this spectrum is not only dominated by BSA peaks. Furthermore, the peaks of the adsorbed BSA on the HAP NPs appear at the same wavenumbers as the peaks of the pristine BSA. Consequently, no peak shift could be observed indicating that the secondary structure of BSA does not alter during adsorption to the HAP NPs. This was also confirmed by Swain, who analyzed BSA adsorbed to HAP with FT-IR.[40]

Composite protein microcapsules

The formation of the thin composite mineral proteinaceous shells was realized with various types of nanoparticles, which were pre-modified with BSA.

The characterization and modification of composite protein microcapsules as well as the mechanism of their formation will be discussed in the following sections. As a control, pristine NPs solely as well as in an immediate combination with BSA without pre-modification were tested for the formation of a Pickering emulsion, which was not successful. The pristine NPs could only form big and unstable oil droplets, while BSA and not pre-modified NPs formed an emulsion but only with seldom NPs sparsely distributed over the capsule shell. We suggest that the free BSA being in competition with the BSA modified NPs is faster at the interface and forms proteinaceous microcapsules. Therefore, the pre-modification of the NPs with BSA is essential for the formation of composite protein–mineral shells. In a further control experiment, the vortexing was chosen as a comminution method to examine whether the treatment with a high-intensity ultrasound is needed to obtain a stable emulsion. Usage of vortex mixing for the emulsion preparation instead of high-intensity ultrasound resulted again in mostly big unstable oil droplets.

Cryo SEM and cryo EDX were used to investigate the capsules morphology, fine structure and composition of their shells with different NPs, where the elemental analysis gives information on the composition of the protein–mineral microcapsules. To visualize the distribution in the protein–mineral capsules EDX mapping was used. Raman spectroscopy was performed to examine the structural conformation of adsorbed BSA in the shell of the oil loaded composite microcapsules synthesized by ultrasound treatment.

The BSA–Ludox Cl microcapsules were synthesized by ultrasound and loaded with three different oils, respectively. The visualization of the capsules done by cryo SEM measurements is shown in Fig. 6.

The cross section of a composite microcapsule, which was loaded with toluene, is shown in Fig. 6(A). The shell of this composite microcapsule consists of individual Ludox Cl NPs and their aggregates forming a thin but almost densely packed particle layer at the oil–water interface.

The intact BSA–Ludox Cl microcapsule loaded with mint oil (Fig. 6B), which is partially imbedded in the matrix, does not exhibit spherical particles in the shell, while the inner shell

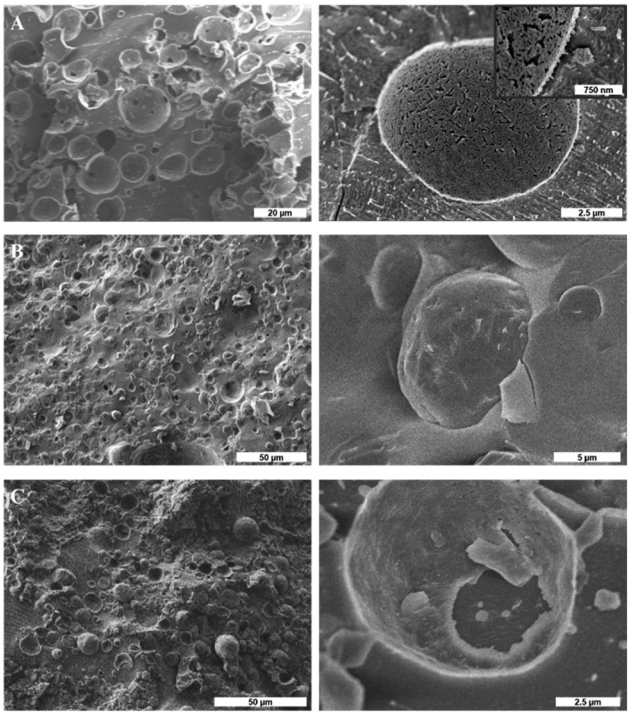

Fig. 6 Cryo SEM images of composite BSA–Ludox Cl microcapsules loaded with different oils: toluene (A), mint oil (B) and Miglyol (C).

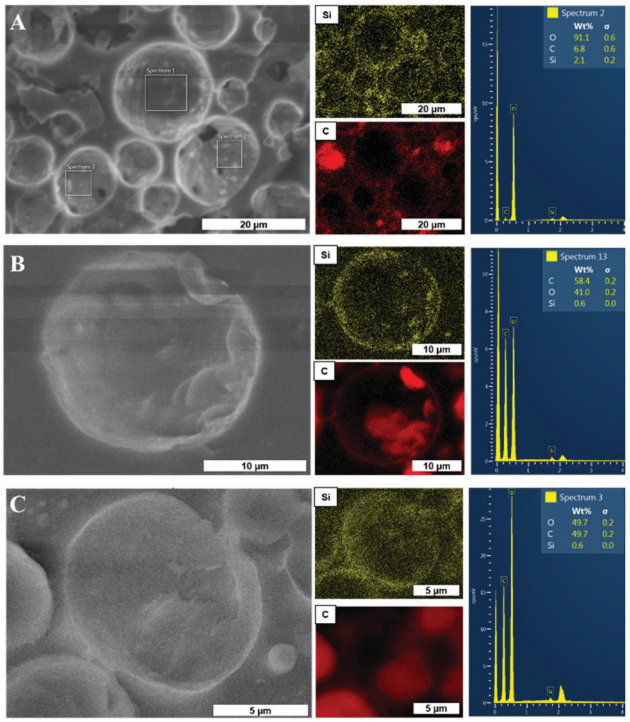

Fig. 7 Cryo SEM images and cryo EDX analysis of composite BSA–Ludox Cl microcapsules loaded with different oils: toluene (A), mint oil (B) and Miglyol (C).

surface shown in the cryo SEM image of the broken composite microcapsule loaded with Miglyol (Fig. 6C) is rather rough.

Notably, the composite microcapsules are larger and more polydisperse than the proteinaceous microcapsules synthesized without NPs. The toluene loaded composite capsules have sizes of 8–13 μm, while the composite capsules loaded with Miglyol and mint oil are slightly smaller with an average size of 5–7.5 μm.

The different oils have different interfacial energies, which also influences the attachment of the NPs at the interfaces of oil droplets and their sizes. However, all composite microcapsules have in common that they are not perfectly spherical shaped and have a rather rough surface.

Since the cryo SEM images only indicate the presence of the Ludox Cl NPs in the capsule shell, cryo EDX mapping of the composite microcapsules was performed for a better visualization of the particle distribution and for detection of the elemental composition. Fig. 7 summarizes the EDX analysis results of BSA–Ludox Cl microcapsules loaded with toluene, mint oil and Miglyol. A cryo SEM image is shown on the left, the corresponding EDX mapping is displayed in the middle of the figure, while an overview of the elemental composition is given on the right. The EDX mapping results show that the shells of all capsules contain an essential amount of silicon (colored yellow) evidencing the presence of silica nanoparticles and their even distribution at the interface. Consequently, the capsules were successfully synthesized with Ludox Cl NPs. Furthermore, the EDX mapping shows the presence of carbon in the same area as silicon was detected caused by the modification of the Ludox Cl NPs with BSA, which is composed of amino acids. Additionally, carbon was detected in large amounts inside of broken capsules as well as in holes in the capsule shell due to residues of the loaded oil. 6.8% carbon and 2.1% silicon were detected in the capsule shell of BSA–Ludox Cl microcapsules loaded with toluene (Fig. 7(A)).

The high amount of oxygen with 91.1% is explained by the cryo measurement method, because the sample was prepared out of the liquid phase. The elemental composition of the microcapsules loaded with mint oil and Miglyol show a much higher amount of carbon with 58.4% and 49.7%, respectively, while the amount of silicon decreased to 0.6% for both types of capsules. Since the analyzed capsules have holes or are broken, this increase in amount of carbon is caused by the residues of the loaded oils.

After the successful synthesis of composite protein microcapsules with a shell consisting of BSA modified Ludox Cl NPs and loaded with three different oils, microcapsules with other NPs (Si71, $CaCO_3$ and HAP) were synthesized. The cryo SEM images of those microcapsules can be seen in Fig. 8. The result of the microcapsule formation with Si71 is shown in Fig. 8(A). The overview cryo SEM image illustrates the broad size distribution while the close-up image exhibits the rough inner shell surface of the BSA–Si71 microcapsule. The size of these capsules is similar to the ones synthesized with Ludox Cl with an average size of 10 μm. However, the BSA–Si71 microcapsules demonstrate rather spheroidal shapes than spherical ones. The largest capsules were synthesized with $CaCO_3$ NPs with an

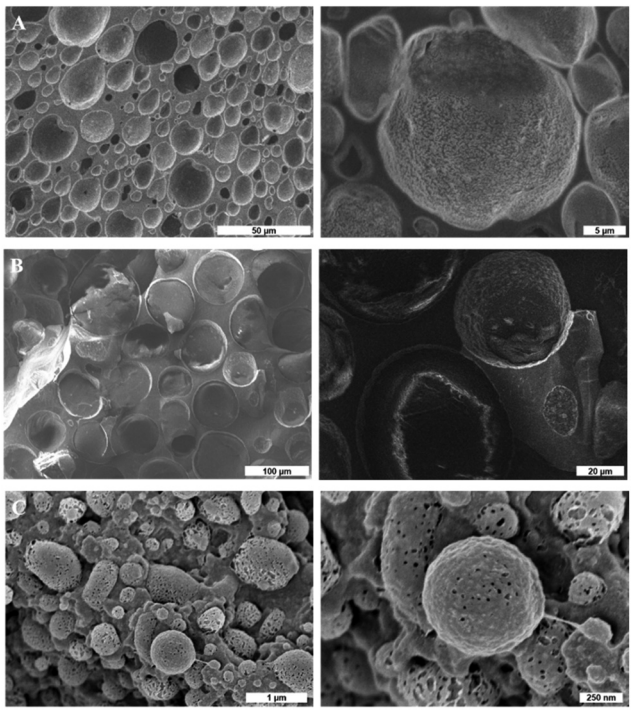

Fig. 8 Cryo SEM images of composite BSA microcapsules loaded with toluene and synthesized with different nanoparticles: Si71 (A), $CaCO_3$ (B) and HAP (C).

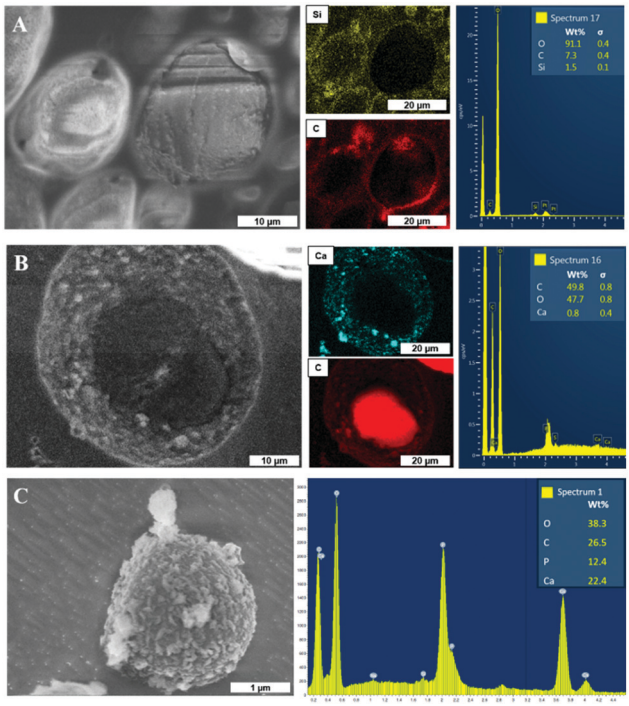

Fig. 9 Cryo SEM images of composite BSA microcapsules loaded with toluene and synthesized with different nanoparticles: Si71 (A), $CaCO_3$ (B) and HAP (C); cryo EDX of capsules (A) and (B) and EDX of dried BSA–HAP microcapsules that were washed three times with a dropping funnel (C).

average size of 50–60 µm. On the surface of these BSA–$CaCO_3$ microcapsules, a roughness can be observed as well (Fig. 8(B)). On the contrary, the composite microcapsules synthesized with HAP NPs were the smallest (Fig. 8(C)).

They exhibit an average size of 1–2.5 µm and in addition to a rough surface, they have numerous holes in the shell. These holes are probably caused by the evaporation of the loaded toluene during the preparation for the cryo SEM measurements. Notably, some of these microcapsules have a cylindrical shape. This shows, that the different NPs have strong influence on the size and shape of the microcapsules as they attach differently at the interface.

For more clarification of what causes this roughness on the shell surface, these capsules were analyzed with cryo EDX as well (see Fig. 9). The EDX mapping and the corresponding elemental composition of the BSA–Si71 microcapsules (Fig. 9(A)) show similar results as seen before for the BSA Ludox Cl microcapsules that were loaded with toluene. Silicon and carbon were detected evenly distributed in the capsule shell. Even the detected amounts of silicon and carbon shown in the elemental composition are in a similar range. Fig. 9(B) shows the EDX mapping of the BSA–$CaCO_3$ microcapsules and as expected calcium and carbon were detected in the carbon shell. Notably, little aggregates are located on the inner shell surface, which are highly cyan colored indicating a high calcium content. On the other hand, the high carbon content in the middle of the broken microcapsule is once more attributed to the residues of the loaded oil causing a highly red colored spot. This is also reflected in the elemental composition showing 49.8% of carbon, while the amount of calcium was 0.8%. The amount of detected NPs is in a similar range as in the broken or holey capsules synthesized with Ludox Cl and loaded with mint oil or Miglyol (Fig. 9).

On the contrary, the EDX analysis of the BSA–HAP microcapsules loaded with toluene was more challenging. It is possible that the content of the incorporated particles was too low and below the detection limit, so that EDX mapping was not successful. Therefore, the BSA–HAP microcapsules were thoroughly washed with a dropping funnel, dried and then analyzed with EDX. The elemental composition proves that the BSA modified HAP NPs are contained in the capsule shell by detecting carbon, phosphorus and calcium in the dried and washed microcapsules.

The spectrum of the dried BSA–Ludox Cl microcapsules that were loaded with toluene is shown in Fig. 10 and for a better comparison the spectra of pristine BSA, Ludox Cl NPs and BSA modified Ludox Cl NPs, which were discussed before, were added as well (Fig. 10A). Moreover, the spectrum of the dried BSA–toluene capsules without NPs was added in the right diagram (Fig. 10B) for better comparison.

The Raman spectra of BSA adsorbed on the Ludox Cl NPs and BSA in the shell of composite microcapsules made of Ludox Cl and BSA are nearly identical, which allows the assumption that the ultrasound treatment at the oil/water interface does not affect the conformational structure of the BSA adsorbed at the NPs surface. The comparison with the spectrum of the BSA microcapsules without NPs confirms that

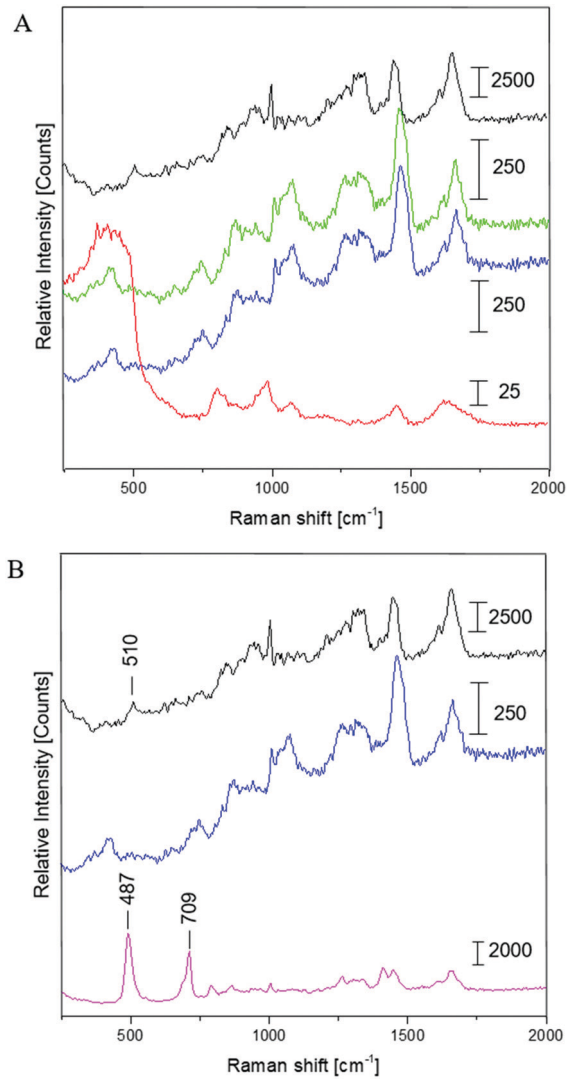

Fig. 10 Raman spectra for: (A) pristine BSA (black), pristine Ludox Cl (red), BSA modified Ludox Cl (green), dried BSA-Ludox Cl capsules loaded with toluene (blue) and (B) dried BSA–toluene-capsules (magenta).

no conformational changes take place due to the absence of the two characteristic peaks of the cross-linked BSA at 487 cm^{-1} and 709 cm^{-1}, which were discussed before.[1]

This examination reveals that the BSA adsorbed on the NPs surface in the shell of the composite microcapsules are not cross-linked by intermolecular disulfide bonds, in contrast to the BSA molecules in the proteinaceous microcapsules made of BSA alone.

Instead, a Pickering-Emulsion formation takes place because of the amphiphilicity-driven spontaneous attachment of the BSA-modified nanoparticles at the oil/water interface. When BSA is adsorbed on the NPs, it is not possible anymore to change its conformation at the oil–water interface in the fashion required for the formation of intermolecular disulfide bonds upon ultrasound treatment. Furthermore, it is likely that the sites of the adsorbed BSA molecule containing the intramolecular disulfide bonds are less accessible to the radicals formed by the ultrasound treatment. Thus, the superoxide radicals are inhibited in the formation of intermolecular disulfide bonds. Fig. 1 displays the mechanism of the synthesis of oil loaded composite BSA microcapsules.

Modification

Proteins can be labelled by dyeing agents, which should contain moieties enabling their detection due to an intrinsic property like fluorescence. The reactive group of the modifying agent links to the functional group of the protein and after this modification the agent is covalently attached resulting in a permanently labelled protein with a unique detectable property. A variety of fluorophores is available for different applications. One of the most popular is fluorescein isothiocyanate (FITC), which is reactive towards nucleophilic sites like amines. Since FITC is able to form stable products with primary amine groups, it is highly selective for N-terminal amines in proteins.

The nucleophile attacks the electrophilic carbon of the isothiocyanate group resulting in the formation of a thiourea bond between the protein and FITC.[41] Fig. 11 shows the BSA–Ludox Cl microcapsules loaded with toluene and modified with FITC. The fluorescence microscopy image visualizes the shell of the composite protein microcapsules consisting of the BSA modified Ludox Cl NPs. Moreover, this shows that the microcapsules can be easily modified *via* the primary amine group of BSA.

However, the silanol groups, Si–OH, on the surface of the Ludox Cl NPs can be easily modified to various functional groups as well by the treatment with different alkoxysilanes. 3-Aminopropyltriethoxysilane (APTES) is one of the most applied alkoxysilanes, which is commonly used for the surface functionalization of silicon oxide surfaces. It can be used as an coupling agent for further functionalization due to its terminal amino group.

During the modification of the Ludox Cl NPs the ethoxy groups of APTES react with the silanol groups on the silica surface to form stable siloxane bonds (Si–O–Si), resulting in ethanol as the leaving group and an aminopropyl-terminated surface.[42,43]

APTES is very sensitive to several reaction conditions.[42,44] Ethoxy groups can be hydrolyzed due to the presence of water in the system and *via* a condensation reaction.

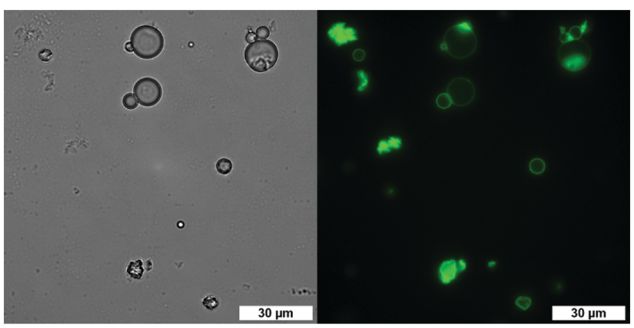

Fig. 11 Microscopy and fluorescence microscopy image of BSA–Ludox Cl microcapsules loaded with toluene and modified with FITC.

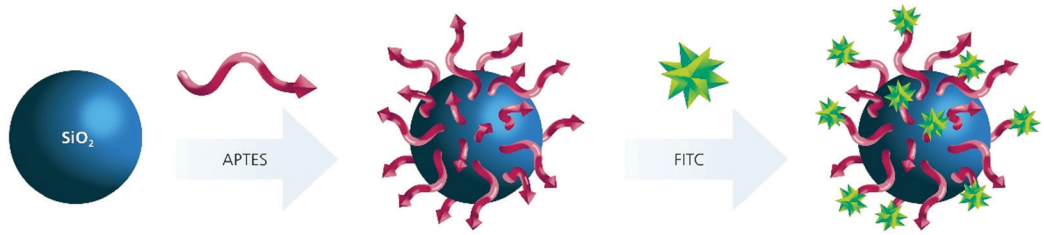

Fig. 12 Illustration of the surface modification of Ludox Cl NPs with APTES and FITC.

Table 2 List of zeta potential values of pristine and modified Ludox Cl nanoparticles at pH = 7

Nanoparticles	Zeta potential [mV]
Ludox Cl	+26.6 ± 0.5
Ludox Cl + APTES	+42.9 ± 1.1
Ludox Cl + APTES + FITC	+29.7 ± 0.9

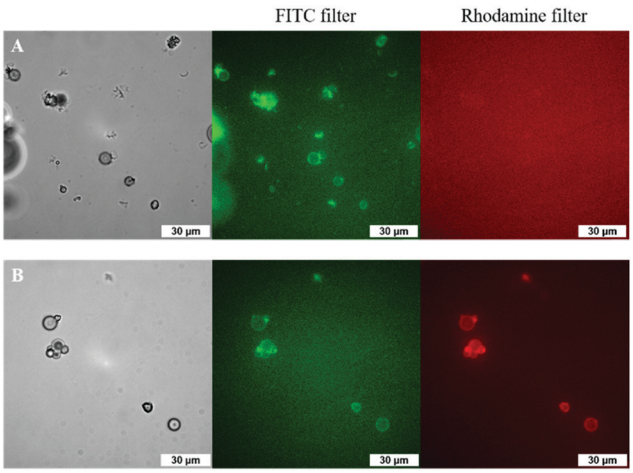

Fig. 13 Microscopy and fluorescence microscopy images of BSA–Ludox Cl microcapsules loaded with toluene that were modified with APTES and FITC (A) and additionally with RITC (B).

The resulting moieties react with each other to produce siloxane bonds leading to a 3D-polymerization. The result of the silanization without water in the system are reaction of only one, two or all three ethoxy groups with the silanol terminated Ludox Cl NPs. The free amine group is pointing towards the liquid phase and is available for further functionalizations.[45] It can be used as linkage unit to attach other functional molecules like FITC by forming thiourea linkage (see Fig. 12).

The modification with APTES increased the positive zeta potential of Ludox Cl, while the further modification with FITC *via* the amine groups resulted in a decrease of the zeta potential (see Table 2). Additionally, these FITC pre-labeled Ludox Cl NPs were modified with BSA as usually and used for the synthesis of composite microcapsules loaded with toluene *via* ultrasonication shown in Fig. 13A. As can be seen in the fluorescence microscopy image, the shell of the successfully synthesized composite microcapsules consists of the Ludox Cl NPs that were modified with APTES, FITC and BSA.

After the successful modification of the composite microcapsules *via* the amine groups of BSA and the silanol groups of the Ludox Cl NPs separately, it was also possible to synthesize capsules that were modified simultaneously *via* BSA and Ludox Cl. For this synthesis BSA was pre-modified with rhodamine B isothiocyanate (RITC) *via* the reaction of the isothiocyanate group with the amino group of BSA (see Fig. 13B). The microscopy images with different filters show clearly the fluorescence of FITC attached to APTES that was bound to the Ludox Cl NPs and of RITC, which is linked to BSA.

Conclusions

We have shown the successful synthesis of oil loaded protein–mineral microcapsules. The results were supported by TGA, zeta potential, EDX and Raman measurements showing that BSA adsorbed strongly on four different types of NPs, which is the result of various interactions between the components, including van der Waals forces, hydrogen bond forces, electrostatic forces and hydrophobic interactions. Furthermore, the cryo SEM images and EDX mapping showed that the microcapsule formation was successful with three different oils and the aforementioned NPs. Both, the loaded oils and the NPs in the capsule shell, had influence on size and shape of the microcapsules. The examination of the composite capsule with Raman revealed that the BSA molecules adsorbed on the NPs surface in the shell of the composite microcapsules are not cross-linked by intermolecular disulfide bonds. This is in contrast with our previous findings of cross-linked BSA molecules in microcapsules made of BSA alone.[1] Instead, a Pickering-Emulsion formation takes place. Additionally, we demonstrated a successful modification of composite microcapsules both through pre-modification of main components and also the post-modification of the surface of ready composite microcapsules.

Conflicts of interest

There are no conflicts to declare.

Acknowledgements

We would like to thank Dr Brigitte Tiersch and Sibylle Rüstig for the SEM images of the microcapsules and Heike Runge for

the SEM images and the EDX analysis. Additionally, we give thanks to Kathrin Geßner for performing the TGA.

Notes and references

1 U. Doering, D. Grigoriev, K. Tapio, S. Rosencrantz, R. R. Rosencrantz, I. Bald and A. Böker, *RSC Adv.*, 2021, **11**, 16152–16157.
2 K. D. Hermanson, D. Huemmerich, T. Scheibel and A. R. Bausch, *Adv. Mater.*, 2007, **19**, 1810–1815.
3 Y. Zhu, W. Tong, C. Gao and H. Möhwald, *J. Mater. Chem.*, 2008, **18**, 1153–1158.
4 W. Tong and C. Gao, *J. Mater. Chem.*, 2008, **18**, 3799–3812.
5 A. P. R. Johnston, C. Cortez, A. S. Angelatos and F. Caruso, *Curr. Opin. Colloid Interface Sci.*, 2006, **11**, 203–209.
6 W. Tong, C. Gao and H. Möhwald, *Colloid Polym. Sci.*, 2008, **286**, 1103–1109.
7 G. Jutz and A. Böker, *J. Mater. Chem.*, 2010, **20**, 4299–4304.
8 H. Chen, J. He, H. Tang and C. Yan, *Chem. Mater.*, 2008, **20**, 5894–5900.
9 H. Maeda, M. Okada, S. Fujii, Y. Nakamura and T. Furuzono, *Langmuir*, 2010, **26**, 13727–13731.
10 D. Lee and D. A. Weitz, *Adv. Mater.*, 2008, **20**, 3498–3503.
11 I. Akartuna, E. Tervoort, A. R. Studart and L. J. Gauckler, *Langmuir*, 2009, **25**, 12419–12424.
12 S. Gouin, *Trends Food Sci. Technol.*, 2004, **15**, 330–347.
13 G. Nelson, *Int. J. Pharm.*, 2002, **242**, 55–62.
14 R. Gref, Y. Minamitake, M. T. Peracchia, V. Trubetskoy, V. Torchilin and R. Langer, *Science*, 1994, **263**, 1600–1603.
15 R. Akiyama and S. Kobayashi, *Chem. Rev.*, 2009, **109**, 594–642.
16 Y. Han, M. Fuji, D. Shchukin, H. Möhwald and M. Takahashi, *Cryst. Growth Des.*, 2009, **9**, 3771–3775.
17 Y. Cai, H. Pan, X. Xu, Q. Hu, L. Li and R. Tang, *Chem. Mater.*, 2007, **19**, 3081–3083.
18 D. W. Green, S. Mann and R. O. C. Oreffo, *Soft Matter*, 2006, **2**, 732–737.
19 K. Samborska, S. Boostani, M. Geranpour, H. Hosseini, C. Dima, S. Khoshnoudi-Nia, H. Rostamabadi, S. R. Falsafi, R. Shaddel, S. Akbari-Alavijeh and S. M. Jafari, *Trends Food Sci. Technol.*, 2021, **108**, 297–325.
20 K. S. Suslick and M. W. Grinstaff, *J. Am. Chem. Soc.*, 1990, **112**, 7807–7809.
21 X. Cui, B. Wang, S. Zhong, Z. Li, Y. Han, H. Wang and H. Moehwald, *Colloid Polym. Sci.*, 2013, **291**, 2271–2278.
22 Q. Ye, M. Biviano, S. Mettu, M. Zhou, R. Dagastine and M. Ashokkumar, *RSC Adv.*, 2016, **6**, 106130–106140.
23 U. Angel (Shimanovich), D. Matas, S. Michaeli, A. Cavaco-Paulo and A. Gedanken, *Chem. – Eur. J.*, 2010, **16**, 2108–2114.
24 Y. Han, D. Radziuk, D. Shchukin and H. Moehwald, *Macromol. Rapid Commun.*, 2008, **29**, 1203–1207.
25 A. Schulz, B. M. Liebeck, D. John, A. Heiss, T. Subkowski and A. Böker, *J. Mater. Chem.*, 2011, **21**, 9731–9736.
26 S. S. Behrens, *J. Mater. Chem.*, 2008, **18**, 3788–3798.
27 I. Yamashita, *J. Mater. Chem.*, 2008, **18**, 3813–3820.
28 J. M. Peula-Garcia, R. Hidaldo-Alvarez and F. J. de las Nieves, *Colloid Polym. Sci.*, 1997, **275**, 198–202.
29 J. Chen, T. He, W. Wu, D. Cao, J. Yun and C. K. Tan, *Colloids Surf., A*, 2004, **232**, 163–168.
30 E. Song, D. Kim, B. J. Kim and J. Lim, *Colloids Surf., A*, 2014, **461**, 1–10.
31 R. Silva, H. Ferreira, N. G. Azoia, U. Shimanovich, G. Freddi, A. Gedanken and A. Cavaco-Paulo, *Mol. Pharmaceutics*, 2012, **9**, 3079–3088.
32 G. S. Deshmukh, S. U. Pathak, D. R. Peshwe and J. D. Ekhe, *Bull. Mater. Sci.*, 2010, **33**, 277–284.
33 I. Galan, F. P. Glasser and C. Andrade, *J. Therm. Anal. Calorim.*, 2013, **111**, 1197–1202.
34 S. Shimabayashi, Y. Tanizawa and K. Ishida, *Chem. Pharm. Bull.*, 1991, **39**, 2183–2188.
35 D. T. H. Wassell, R. C. Hall and G. Embery, *Biomaterials*, 1995, **16**, 697–702.
36 M. Iosin, V. Canpean and S. Astilean, *J. Photochem. Photobiol., A*, 2011, **217**, 395–401.
37 Q. Li, B. Mihailova, D. Creaser and J. Sterte, *Microporous Mesoporous Mater.*, 2001, **43**, 51–59.
38 C. E. Giacomelli and W. Norde, *J. Colloid Interface Sci.*, 2001, **233**, 234–240.
39 W. Norde and J. P. Favier, *Colloids Surf.*, 1992, **64**, 87–93.
40 S. K. Swain and D. Sarkar, *Appl. Surf. Sci.*, 2013, **286**, 99–103.
41 N. Barbero, C. Barolo and G. Viscardi, *World J. Chem. Educ.*, 2016, **4**, 80–85.
42 R. M. Pasternack, S. Rivillon Amy and Y. J. Chabal, *Langmuir*, 2008, **24**, 12963–12971.
43 R. G. Acres, A. V. Ellis, J. Alvino, C. E. Lenahan, D. A. Khodakov, G. F. Metha and G. G. Andersson, *J. Phys. Chem. C*, 2012, **116**, 6289–6297.
44 E. T. Vandenberg, L. Bertilsson, B. Liedberg, K. Uvdal, R. Erlandsson, H. Elwing and I. Lundström, *J. Colloid Interface Sci.*, 1991, **147**, 103–118.
45 C.-H. Chiang, N.-I. Liu and J. L. Koenig, *J. Colloid Interface Sci.*, 1982, **86**, 26–34.